JGR Oceans

RESEARCH ARTICLE
10.1029/2018JC014839

Special Section:
Recent Progresses in Oceanography and Air-Sea Interactions in Southeast Asian Archipelago

Observation of Enhanced Nonlinear Interactions After Severe Tropical Storm Chanchu (2004) in the Western South China Sea

Chang-Rong Liang[1], Gui-Ying Chen[1], Xiao-Dong Shang[1], Xiao-Hui Xie[2], and Dong-Xiao Wang[1]

[1]State Key Laboratory of Tropical Oceanography, South China Sea Institute of Oceanology, Chinese Academy of Sciences, Guangzhou, China, [2]State Key Laboratory of Satellite Ocean Environment Dynamics, Second Institute of Oceanography, State Oceanic Administration, Hangzhou, China

Key Points:
- This study presents the effect of tropical cyclone on the internal wave field
- This study observes enhanced self-interaction of near-inertial waves induced by tropical cyclone
- This study observes enhanced nonlinear interaction among internal tides induced by tropical cyclone

Correspondence to:
X.-D. Shang,
xdshang@scsio.ac.cn

Citation:
Liang, C.-R., Chen, G.-Y., Shang, X.-D., Xie, X.-H., & Wang, D.-X. (2019). Observation of enhanced nonlinear interactions after severe tropical storm Chanchu (2004) in the western South China Sea. *Journal of Geophysical Research: Oceans*, *124*, 3837–3848. https://doi.org/10.1029/2018JC014839

Received 9 JAN 2019
Accepted 8 MAY 2019
Accepted article online 10 MAY 2019
Published online 13 JUN 2019

Abstract Severe tropical storm Chanchu passed the subsurface mooring in the western South China Sea in June 2004, and its effects on the internal wavefield and nonlinear interactions were examined. The internal wavefield was characterized by diurnal (D_1) and semidiurnal (D_2) tides before Chanchu. However, after the passage of Chanchu, the internal wavefield was not only characterized by diurnal and semidiurnal tides but also by near-inertial (f) waves, internal waves with higher harmonic frequency ($fD_2 = f+D_2$ and $D_3 = D_1+D_2$), and enhanced diurnal currents. Analysis of the rotary coefficient and bicoherence suggested that the observed fD_2 waves, D_3 waves, and enhanced diurnal currents originated from the nonlinear interactions of $f+D_2 = fD_2$, $D_1+D_2 = D_3$, and $f+f = 2f$, respectively. Previous studies indicated that the nonlinear interactions induced by tropical cyclones mainly occur between the near-inertial waves and internal tides ($f+D_1 = fD_1$ or $f+D_2 = fD_2$). Our observations indicate that tropical cyclones can also induce the self-interaction of near-inertial waves ($f+f = 2f$) and enhance nonlinear interactions between diurnal and semidiurnal tides ($D_1+D_2 = D_3$). Critical diurnal latitudes (where $2f \approx D_1$) play an important role in the occurrence of these nonlinear interactions. Near-inertial waves undergo self-interactions ($f+f = 2f$) near the critical diurnal latitudes, and near-inertial energy is transferred to diurnal waves. Enhanced diurnal waves further contribute to the nonlinear interactions of $D_1+D_2 = D_3$. These nonlinear processes might promote the energy cascade of the near-inertial waves induced by tropical cyclones near the critical diurnal latitudes and play an important role in ocean mixing.

1. Introduction

Near-inertial waves, namely internal waves with a frequency near the local inertial frequency ($=2\Omega \sin \phi$, where $\Omega = 7.2921 \times 10^{-5}$ rad/s is the local vertical component of the Earth's rotation vector and ϕ is the latitude), are often observed in the ocean. These waves form the energetic part of the internal wave spectrum (Ferrari & Wunsch, 2009; Garrett & Munk, 1975). Surface wind forcing has long been suggested to be a dominant mechanism for the generation of near-inertial waves (Garrett, 2001; Gill, 1984). As a result, the largest velocity amplitude they cause is often observed in the upper ocean and can reach 2 m/s (Sanford et al., 2007; Sanford et al., 2011; Teague et al., 2007). The near-inertial waves generated in the upper ocean generally persist for a dozen days before decay (D'Asaro, 1989; Garrett, 2001; Qi et al., 1995). Nonlinear interactions are an important mechanism for the decay of near-inertial waves, as they are the first step in the cascade of energy to shorter wavelengths and eventually to ocean mixing. Previous numerical experiments and observations (Davies & Xing, 2003; van Haren et al., 1999; van Haren et al., 2002; Xie et al., 2008; Xing & Davies, 2002) indicated that nonlinear interactions can cascade energy from near-inertial waves and internal tides into small-scale internal waves.

The South China Sea (SCS), one of the largest marginal seas in the Pacific Ocean, covers the area from approximately 0 to 23°N and 100 to 120°E. A dozen tropical cyclones (TCs) pass through or form in this marginal sea each year (Goh & Chan, 2010; Wang et al., 2007), which can induce energetic near-inertial waves, and provide high levels of energy for ocean mixing (Xu et al., 2013). There have been several observational studies of near-inertial waves induced by TCs in the SCS (Cao et al., 2018; Chen et al., 2013; Guan et al., 2014; Sun et al., 2011). Sun et al. (2011) explored the evolution of near-inertial waves during a severe tropical storm in the western SCS and explained the causes of a blue shift in the inertial frequency.

Chen et al. (2013) examined the seasonal variability of near-inertial waves and their relation to TCs and eddies in the northwestern SCS. Guan et al. (2014) reported the response of the upper ocean to typhoon in the northern SCS, while Cao et al. (2018) explored the features of typhoon-induced near-inertial waves and their underlying mechanisms with mooring array data. These studies have greatly increased our knowledge of near-inertial waves induced by TCs in the SCS. However, the effects of TCs on the internal wavefield and nonlinear interactions are still not fully understood. Although numerical experiments (Simmons, 2008; Xing & Davies, 2002) have found that nonlinear interactions can cascade energy from near-inertial waves and internal tides into higher-mode internal waves, few observational studies have reported these nonlinear processes after the passage of TCs, especially near the critical diurnal latitudes. One observational study involving the TC-induced nonlinear interactions in the SCS was reported by Guan et al. (2014). Using mooring data obtained from the northern SCS, Guan et al. (2014) found strong nonlinear interactions between near-inertial waves and diurnal tides after the passage of typhoon. However, to the best of our knowledge, no observational studies have reported the TC-induced nonlinear interactions near the critical diurnal latitudes of the SCS. The critical diurnal latitude band is a special zone for diurnal tides where they are prone to undergo parametric subharmonic instability (PSI, Alford et al., 2007; Alford, 2008; Simmons, 2008; Xie et al., 2009). The effects of the critical diurnal latitudes on the nonlinear interactions and the types of waves that involve nonlinear interactions after the passage of TCs near the critical diurnal latitudes are unclear. The objective of this paper is to investigate the effects of a severe tropical storm on the internal wavefield and demonstrate the enhancement of nonlinear interactions between the internal waves near the critical diurnal latitudes. Nonlinear interactions induced by TCs near the critical diurnal latitudes were found to differ from those occurring in regions far away from the critical diurnal latitudes. In addition to the nonlinear interactions between the near-inertial waves and internal tides, we found that TCs can also induce the self-interactions of near-inertial waves and nonlinear interactions between diurnal and semidiurnal tides near the critical diurnal latitudes. In the following section, we describe the instruments and measurement techniques we used, and the severe tropical storm passing through the observation site. The rotary analysis and bicoherence methods are introduced in section 3. In section 4, we investigate the distribution of energy in the internal wave band with the rotary spectrum and diagnose the nonlinear interactions with bicoherence. Finally, discussion and conclusions are presented in section 5.

2. Mooring Observations

On 26 May 2004, one acoustic Doppler current profiler (ADCP) mooring was deployed in the western SCS to study ocean circulation and internal waves (Figure 1). The mooring was deployed for 123 days from 26 May to 27 September 2004 and provided a detailed description of the internal wavefield. The mooring station was located at 13.99°N and 110.52°E, which is close to the critical bidiurnal latitudes (13.44°N for O_1 internal tide and 14.52°N for K_1 internal tide). The water depth is approximately 1,800 m. The mooring was equipped with an upward looking 75-kHz ADCP that pinged and recorded currents at 30-min intervals with a vertical resolution of 8 m between 8 and 480 m. The ADCP relies on sufficient natural scatters in the water column to create a good return signal. Data with a signal-to-noise ratio below 6 dB were rejected, and the occasional unrealistic extreme values (speed>10 m/s) were removed. If these absent data points had good values adjacent in either time or space, then they were estimated by linear interpolation. The data in the upper 48 m were excluded from analysis as their quality was poor and they could not be easily restored.

One of the TCs that passed through the SCS in 2004 was named Chanchu (Figure 1), which formed in the western Pacific and developed into a severe tropical storm in the SCS. Chanchu arrived at the mooring on 12 June 2004 (yearday 163) with a maximum wind speed of approximately 30 m/s. Details of Chanchu's track and maximum wind speed were obtained from the Typhoon Online website (http://www.typhoon.org.cn/). To explore the effects of Chanchu on the internal wavefield and nonlinear interactions, current data captured by the mooring from 27 May to 8 August 2004 (yeardays 147 to 220) were used for analysis.

3. Spectrum Analysis

Based on the rotary analysis of the vector time series (Gonella, 1972; Thomson & Emery, 2014), the horizontal velocity vector $\boldsymbol{u}(t) = u(t)+iv(t)$ for a specified frequency ω can be separated into clockwise (A_-) and

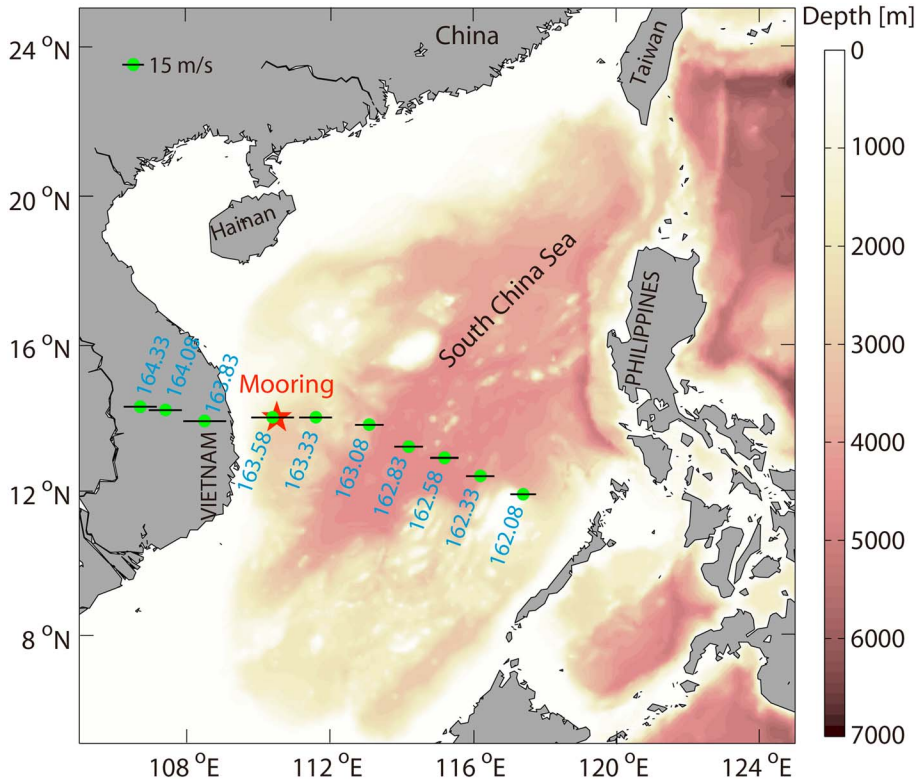

Figure 1. Bottom topography (ETOPO2v2) of the SCS. The location of the ADCP mooring is marked by the red star at 13.99°N, 110.52°E. The track of Chanchu is indicated by the green circles with labeled yeardays (162.08, 162.33, 162.58, ...). The maximum wind speeds are indicated by the scaled horizontal bars. SCS = South China Sea; ADCP = acoustic Doppler current profiler.

anticlockwise (A_+) rotating circular components. One ratio that can be used to describe the polarization characters of the internal waves is the rotary coefficient, which is defined as

$$C_R(\omega) = \frac{A_- - A_+}{A_+ + A_-} \tag{1}$$

C_R is equal to 1, 0, and −1 for clockwise, unidirectional, and anticlockwise motions, respectively. Under linear perturbation, the theoretical rotary coefficient can be defined as (Gonella, 1972; van Haren, 2003)

$$C_R(\omega) = \frac{2\omega f}{\omega^2 + f^2}, \tag{2}$$

where f is the inertial frequency. $C_R = 1$ when ω is equal to f, indicating that inertial waves are clockwise rotary in the Northern Hemisphere. C_R decreases as ω increases in the internal wave band.

The bispectrum is often used to study the nonlinear interactions between internal waves, which is defined as (Kim & Powers, 1979)

$$B(\omega_1, \omega_2) = E\left[A(\omega_1)A(\omega_2)A^*(\omega_1 + \omega_2)\right], \tag{3}$$

where $A = A_+ + A_-$, A^* represents the complex conjugate of A, and $E[\ ]$ is the expected value. Specifically, nonlinear interactions are associated with nonzero value of the bicoherence that is given by

$$b(\omega_1, \omega_2) = \frac{|B(\omega_1, \omega_2)|}{\left\{E\left[|A(\omega_1)A(\omega_2)|^2\right]E\left[|A(\omega_1 + \omega_2)|^2\right]\right\}^{1/2}}. \tag{4}$$

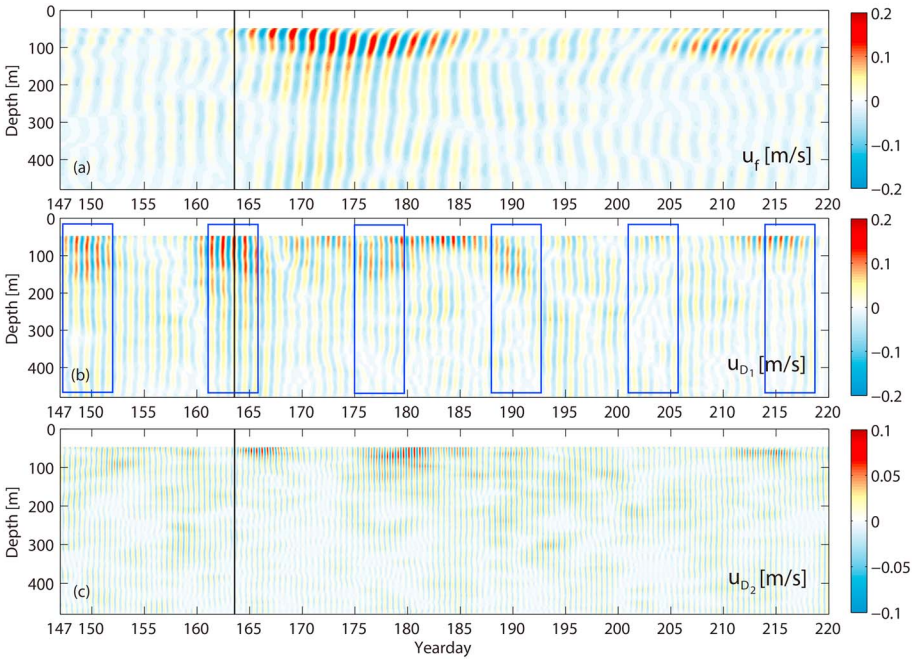

Figure 2. Time series of the (a) u_f, (b) u_{D_1}, and (c) u_{D_2} band-pass-filtered velocities measured by the mooring ADCP from yeardays 147 to 220. In all panels, the vertical black lines represent the time at which Chanchu passed the mooring. The blue rectangles in Figure 2b indicate the periods of spring tides. SCS = South China Sea; ADCP = acoustic Doppler current profiler.

Bicoherence is a quantity that shows whether or not a statistically dominant phase relationship exists for a wave triad that stands out above random phasing (Kim & Powers, 1978, 1979). That is, if waves present at frequencies ω_1, ω_2, and $\omega_1+\omega_2$ are spontaneously excited independent waves, each wave may be characterized by statistically independent random phases. The statistical averaging in equation (4) will lead to a bicoherence value of zero due to the random phase mixing effect. In contrast, if the three spectral components are nonlinearly coupled to each other, the total phase of three waves will not be random. The statistical averaging in equation (4) will lead to a nonzero bicoherence value.

A nonzero bicoherence value generally identifies two components of a nonlinear triad interaction, but for a finite-length time series, even a process with truly independent Fourier components will have a nonzero bicoherence value (Elgar & Guza, 1988). The significance levels of bicoherence must be known to determine if the data are statistically consistent with a linear random phase process. Elgar and Guza (1988) demonstrated that the significance levels of bicoherence can be determined by the number of degrees of freedom (λ). The significance levels of 80%, 90%, and 95% are equal to $\sqrt{3.2/\lambda}$, $\sqrt{4.6/\lambda}$, and $\sqrt{6.0/\lambda}$, respectively, where λ is two times the independent realizations.

4. Results

4.1. Time Series

The observed velocities contain internal waves and mesoscale motions. To clearly show the vertical structure of the internal waves, waves associated with the dominant internal wave frequencies were isolated using a fourth-order Butterworth filter. The filter bounds were $[0.85f, 1.15f]$ for near-inertial waves (f), $[0.9O_1, 1.1K_1]$ for diurnal tides (D_1), and $[0.9M_2, 1.1M_2]$ for semidiurnal tides (D_2), where O_1 and K_1 are the frequencies of lunar diurnal tides and M_2 is the frequency of the principal lunar semidiurnal tide. Figure 2a presents the time series of band-pass-filtered inertial velocity (east-west component). The severe tropical storm Chanchu arrived at the mooring on yearday 163 with a maximum wind speed of approximately 30 m/s (Figure 1). Near-inertial waves induced by Chanchu can be clearly observed in the upper ocean, which were generated in the surface layer and propagated down to the deeper layers. The waves grew in strength from yeardays 163 to 172, during which the amplitude of the near-inertial waves gradually increased from the

background value of 0.05 m/s to a maximum value of approximately 0.2 m/s. The amplitude of the near-inertial waves decreased with an *e*-folding decay timescale of approximately 2 weeks, which is consistent with previous observations (Guan et al., 2014; Oey et al., 2008; Qi et al., 1995). These near-inertial waves exhibited upward phase propagation, suggesting downward energy propagation. Near-inertial signals dominated by downward phase propagation were observed on yeardays 185–200 at depths of 100–400 m (Figure 2a), which contrast with the features of the near-inertial waves induced by Chanchu (upward phase propagation). Furthermore, a phase difference in the velocity signals of approximately 180° occurred alternately on yeardays 185–200 at depths of 100–400 m, exhibiting a *checkerboard* pattern. These distinguishing features suggest that the near-inertial waves may have been generated via PSI (Alford et al., 2007; Xie et al., 2009), as the mooring was located near the critical diurnal latitudes where diurnal tides are prone to undergo PSI (Alford, 2008; Simmons, 2008). However, these near-inertial waves were much weaker than those induced by Chanchu.

Figures 2b and 2c show the time series of the band-pass-filtered diurnal and semidiurnal velocities, respectively. Large velocities for both frequency bands were observed in the upper 200 m. Diurnal tides were stronger and more variable than semidiurnal tides, and the fortnightly spring-neap tidal cycle was apparent in the diurnal signals but faint in the semidiurnal signals. Large-amplitude diurnal velocities were mainly observed during spring tides. However, diurnal waves were enhanced during neap tides when the near-inertial waves were strong (from yeardays 163 to 192). These diurnal enhancements were mainly concentrated in the upper layer. To explore the effects of Chanchu on the internal wavefield and nonlinear interactions, we divided the observation into three stages. Stage 1 ranges from yeardays 147 to 163, corresponding to the period during which the internal wavefield was undisturbed by Chanchu. Stage 2 ranges from yeardays 163 to 192, corresponding to the period of strong near-inertial waves induced by Chanchu. Finally, Stage 3 ranges from yeardays 192 to 220, corresponding to the period during which the near-inertial waves induced by Chanchu had decayed.

4.2. Kinetic Energy Spectra

To consider the energy content as a function of frequency, kinetic energy spectra (clockwise plus anticlockwise) are presented in Figure 3. The kinetic energy spectra are vertically averaged over depths between 48 and 152 m, as the strong near-inertial waves mainly occurred in the upper ocean (Figure 2a). During Stages 2 and 3, the peaks at f band are found at $\omega = 0.516$ cpd (Figure 3b) and $\omega = 0.539$ cpd (Figure 3c), respectively. These peaks are *blue shifted* relative to the local inertial frequency of 0.485 cpd. With the kinetic energy spectrum from Stage 1 (Figure 3a), we examined the background of the internal wavefield for an ocean undisturbed by Chanchu. The kinetic energy spectrum only shows significant peaks at D_1 and D_2 bands. The diurnal tides were the dominant constituents. The peak at f band is smaller than those at D_1 and D_2 bands. The energy density ratio of near-inertial waves to diurnal tides is only 1:3, suggesting that the near-inertial waves before the passage of Chanchu were weak. Small peaks (below the 95% statistical significance level) at fD_1, fD_2, and D_3 bands suggest the absence of fD_1, fD_2, and D_3 waves before the passage of Chanchu. The kinetic energy spectrum of Stage 2 exhibits different features (Figure 3b). This kinetic energy spectrum not only shows significant peaks at D_1 and D_2 bands but also at f band. The ratio of energy density at f, D_1, and D_2 bands is 13:3:1, indicating that near-inertial waves were the dominant constituents. The peak energy density at f band is 0.14 $m^2 \cdot s^{-2} \cdot cpd^{-1}$, which is approximately 20 times larger than that in Stage 1. The increasing energy in the near-inertial waves mainly results from the response of the ocean to Chanchu. The significant peaks at fD_2 and D_3 bands are of particular interest. These peaks are 5 to 6 times more energetic than the background continuum that has a consistent roll-off with that expected for the Garrett-Munk spectrum (Garrett & Munk, 1979). The kinetic energy spectrum for Stage 3 (Figure 3c) only shows significant peaks at f, D_1, and D_2 bands, but no significant peaks are found at fD_1, fD_2, and D_3 bands. The energy density ratio of f, D_1, and D_2 bands is 10:3:1. Near-inertial waves were still the dominant constituents, but they were much weaker than those in Stage 2. These inertial energy levels might result from other wind forcing occurring on yeardays 205–215 (Figure 2a).

The most notable feature of Figure 3 is that significant peaks at fD_2 and D_3 bands are only found in the kinetic energy spectrum of stage 2. fD_2 ($=f+D_2$) is a harmonic of f and D_2, and D_3 ($=D_1+D_2$) is a harmonic of D_1 and D_2. It is noteworthy that the Eulerian records of ocean quantities typically suffer from *fine-structure contamination* wherein the intrinsic spectrum is Doppler shifted by the (vertical) advective motions caused

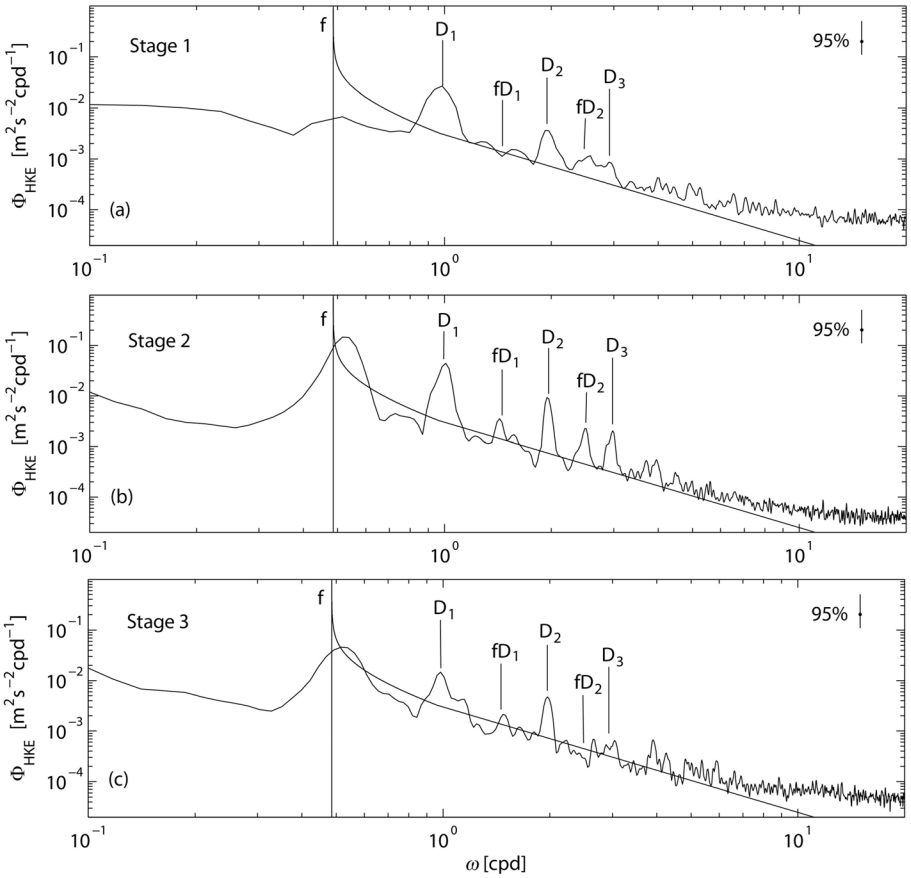

Figure 3. Average rotary spectra (clockwise plus anticlockwise) of the kinetic energy between 48 and 152 m for Stages (a) 1, (b) 2, and (c) 3. The smoothing curves represent the spectral shape predicted by the Garrett and Munk model. The vertical bars represent the frequencies of near-inertial waves (f), diurnal tides (D_1), semidiurnal tides (D_2), and higher harmonics ($fD_1 = f+D_1$, $fD_2 = f+D_2$, and $D_3 = D_1+D_2$). The vertical lines in the upper right-hand corner represent the 95% statistical significance level.

by internal tides and thus shows peaks at $f \pm D_1$ and $f \pm D_2$ bands (Alford, 2001). The possibility of fine-structure contamination can be ruled out in our observation. If the velocity records suffered from fine-structure contamination during the observation, the peak at fD_1 band would be more significant as the diurnal tides were stronger than the semidiurnal tides. However, the peak at fD_2 band is more significant than that at fD_1 band, which is not consistent with the features of the spectrum that suffered from fine-structure contamination. Similarly, the peak at D_3 band is not due to fine-structure contamination. The peak at D_3 band would appear in the spectra of the three stages if the velocity records suffered from fine-structure contamination because both semidiurnal and diurnal tides were strong in all stages. However, significant peak at D_3 band is only observed in the spectrum of Stage 2. Therefore, the peaks at fD_2 and D_3 bands are not due to fine-structure contamination. This suggests that fD_2 and D_3 waves were generated in Stage 2. These waves are likely to be derived from nonlinear interactions between the near-inertial waves and internal tides.

4.3. Shear Spectra and $C_R(\omega)$ Spectra

The features of internal waves derived from nonlinear interactions differ from those of spontaneously formed linear internal waves. Internal waves derived from nonlinear interactions are generally in high modes and have strong shear (Davies & Xing, 2003; van Haren et al., 1999; Xing & Davies, 2002). To explore the features of the observed waves, we compared the shear spectra of the three stages (Figure 4). A vertical interval of 8 m is used for the shear calculation ($\boldsymbol{S} = u_z + iv_z$), and the shear spectra are vertically averaged over depths between 48 and 152 m. No significant peaks are found at fD_2 and D_3 bands in shear spectra of

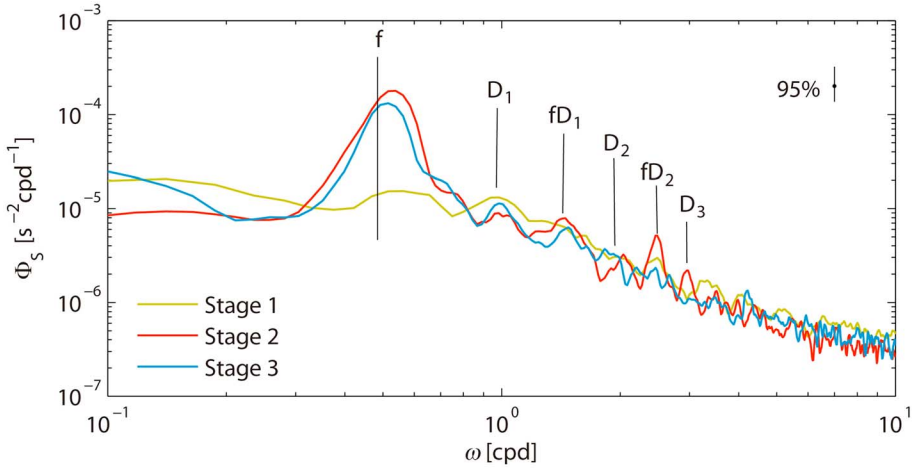

Figure 4. Average rotary spectra (clockwise plus anticlockwise) of the shear between 48 and 152 m for Stages 1, 2, and 3. The vertical lines represent various frequency bands (f, D_1, fD_1, ...), and the vertical line in the upper right-hand corner represents the 95% statistical significance level.

Stages 1 and 3 due to the absence of fD_2 and D_3 waves. In contrast, the shear spectrum of Stage 2 exhibits peaks at fD_2 and D_3 bands, indicating that the fD_2 and D_3 waves observed in Stage 2 had strong shear. This is consistent with the internal waves derived from the nonlinear interactions. Energy can be transferred from large-scale (low-mode) to small-scale (high-mode) internal waves through nonlinear interactions (Davies & Xing, 2003; van Haren et al., 1999; Xing & Davies, 2002).

To further confirm the occurrence of nonlinear interactions, we examined the polarization characteristics of the internal waves with the $C_R(\omega)$ spectrum (Figure 5). If fD_2 waves were the nonlinear coupling waves derived from nonlinear interactions between near-inertial waves and diurnal tides, their polarization characteristics should be strongly clockwise, as those of the near-inertial waves are (Mihaly et al., 1998; van Haren, 2003). The observed C_R exhibits a strong predominance of clockwise waves near the inertial frequency, as expected in linear wave theory for the Northern Hemisphere. Theoretically, C_R decreases as ω increases within the internal wave band if the internal waves were linearly independent (equation (2)). The C_R values of Stage 1 are almost consistent with the theoretical values except those near f band. The C_R values near f band are much lower than the theoretical values. This is mainly due to the lack of near-inertial variability during this stage. The C_R values of Stage 3 are also consistent with the theoretical values and exhibit a decreasing trend as predicted by the theory. No significant peak that deviates largely from the theoretical value is found in the spectra of Stages 1 and 3. However, the C_R values of Stage 2 do not show a smooth decrease with frequency, as predicted by the theory. Instead, there is an elevated peak at fD_2 band. This peak value reaches 0.65, which is significantly greater than the theoretical value of 0.38. The large C_R

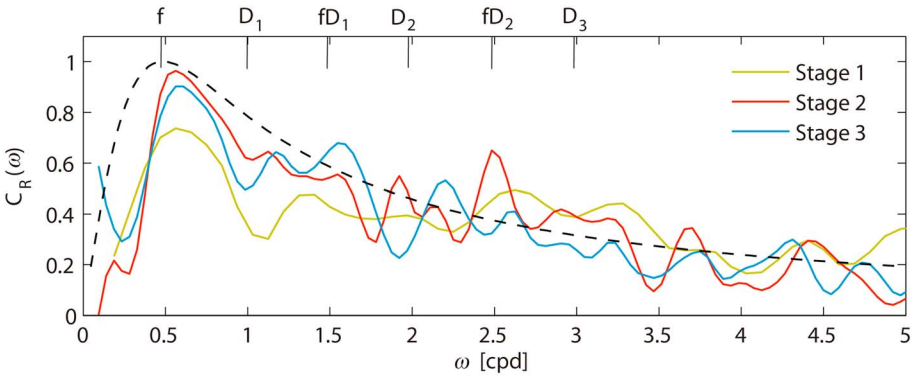

Figure 5. Moderately smoothed rotary coefficient. The dashed curve is the variation in the theoretical rotary coefficient. The vertical lines represent various frequency bands (f, D_1, fD_1, ...).

value at fD_2 band suggests that the fD_2 waves were strongly clockwise, which is consistent with the polarization characteristics of near-inertial waves. These observations indicated that the observed fD_2 waves in Stage 2 were forced by the near-circular clockwise near-inertial waves, rather than spontaneously formed.

4.4. Diurnal Currents, fD_2, and D_3 Waves

The above spectrum analysis indicates that enhanced diurnal currents, fD_2 waves, and D_3 waves occurred during the stage characterized by strong near-inertial waves induced by Chanchu. The relationship between these enhanced waves and near-inertial waves can be also observed in the temporal domain. Strong diurnal currents were only observed during spring tides in Stages 1 and 3, while strong diurnal currents were observed during both spring and neap tides in Stage 2 (Figure 2b). The diurnal enhancements during neap tides in Stage 2 were mainly concentrated in the upper 150 m, with the largest amplitude reaching 0.18 m/s, which is comparable to the amplitude during spring tides. These observations suggest that the enhanced diurnal currents observed in Stage 2 were strongly related to the near-inertial waves induced by Chanchu.

Figures 6a and 6b show time series of the meridional velocities of f and fD_2 bands, respectively. Elevated fD_2 waves were observed during Stage 2, and their maximum amplitude approached 0.10 m/s, which is comparable to the amplitude of semidiurnal tides (Figure 2c). Not all of the strong near-inertial waves were accompanied by elevated fD_2 waves; only the strong near-inertial waves on yeardays 174–181 were (indicated by the red rectangle). This suggests that, in addition to the near-inertial waves, other factors must be met in the generation of fD_2 waves. Numerical models (Davies & Xing, 2003; Xing & Davies, 2002) have indicated that nonlinear terms $w\partial u_f/\partial z$ and $w\partial v_f/\partial z$ play an important role in the nonlinear processes, where w is the vertical velocity caused by internal tides, and $\partial u_f/\partial z$ and $\partial v_f/\partial z$ are the shear from near-inertial waves. Here we cannot examine the relationship between fD_2 waves and nonlinear terms directly owing to the lack of vertical velocity data. However, we can calculate the near-inertial shear $|S_f| = (|\partial u_f/\partial z|^2+|\partial v_f/\partial z|^2)^{1/2}$ and examine its relation to the fD_2 waves. The time series of near-inertial shear is shown in Figure 6c. fD_2 waves are found to be strongly related to the near-inertial shear. fD_2 waves were concentrated within the upper 130 m, where near-inertial shear is strong (indicated by the red rectangle), suggesting that near-inertial shear plays an important role in the generation of fD_2 waves. These observations are consistent with the model created by Xing and Davies (2002) whose results indicate that the enhanced energy at inertia-tidal interaction frequencies ($f+D_2$) is mainly caused by the strong inertial shear aroused by inertial waves.

The relationship between D_3 and near-inertial waves can also be observed in the temporal domain. Figures 6d and 6e show time series of the kinetic energy of near-inertial and D_3 waves, respectively. The kinetic energy is given by $E = 0.5\rho_0(u^2+v^2)$, where $\rho_0 = 1024$ kg/m^3 is the reference water density. Similar to fD_2 waves, not all of the strong near-inertial waves were accompanied by D_3 waves, which are also related to the near-inertial shear. Elevated D_3 waves were mainly concentrated in the upper 150 m, where the near-inertial shear was strong (indicated by the red rectangle). Good relationships between D_3 waves, near-inertial waves, and near-inertial shear suggest that the near-inertial waves and shear induced by Chanchu play an important role in the generation of D_3 waves.

The near-inertia waves experienced great evolution during Stage 2 (Figure 6d). The near-inertial waves on yeardays 163–173 were stable, with most of the energy concentrated at depths of 50 to 75 m. However, they became unstable after yearday 173. The near-inertial energy scattered to a deeper depth (50–130 m) and decayed quickly on yeardays 173–181 (indicated by the green curve in Figure 6d). The scattering and decay of energy occurred at the same depth-time range as elevated fD_2 and D_3 waves (indicated by the red rectangle), which suggests that the near-inertial waves might endure nonlinear interactions after yearday 173, and near-inertial energy was transferred to higher-frequency internal waves. Wave radiation (including lateral and downward radiation) can also cause near-inertial waves to decay (D'Asaro, 1989; Garrett, 2001). However, we have no more data to estimate the energy that radiates away and the energy transferred to higher-frequency internal waves.

4.5. Bicoherence

To further confirm that the diurnal currents, fD_2 waves, and D_3 waves observed in Stage 2 are the nonlinear coupling waves derived from nonlinear interactions, we diagnose the internal wavefield using bicoherence

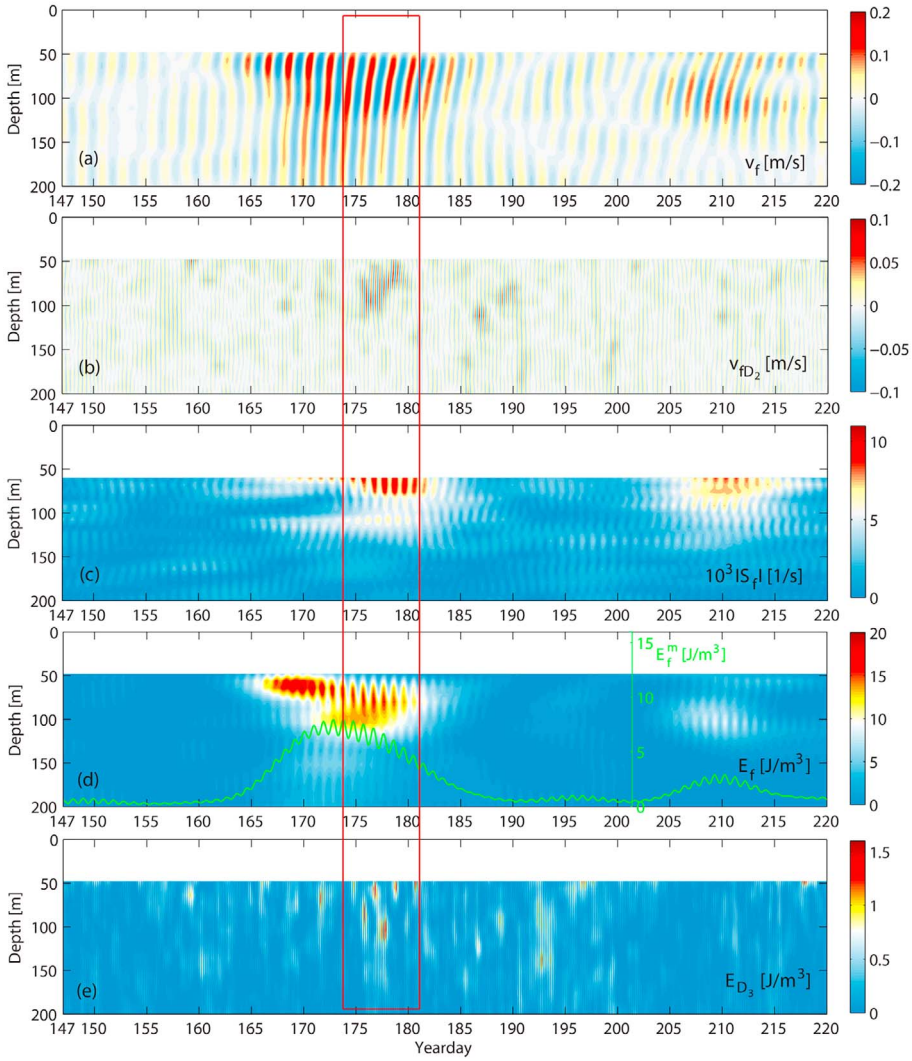

Figure 6. Time series of (a) near-inertial velocity, (b) fD_2 velocity, (c) near-inertial shear, (d) kinetic energy of the near-inertial waves, and (e) kinetic energy of the D_3 waves. The green curve in Figure 6d represents the average kinetic energy of the near-inertial waves between 48 and 200 m. In all panels, the red rectangle indicates the period of elevated fD_2 and D_3 waves.

spectra. The velocity data in Stage 2 were divided into seven segments (50% overlapping) for the bicoherence calculation. We assumed that the two velocity components were dependent and did not increase the degrees of freedom. Thus, the seven independent realizations suggest that the number of degrees of freedom is 14, and the significance levels of 90% and 95% are equal to 0.573 and 0.655, respectively. Figure 7a provides the average bicoherence of velocities $u(t)$ and $v(t)$ from the depth bins between 72 and 96 m. Large bicoherence values are found near the frequency pairs of $[f, f] = [0.485, 0.485]$, $[f, D_2] = [0.485, 1.932]$, and $[D_1, D_2] = [1.003, 1.932]$ cpd, which are significant at the 90% level, indicating the occurrence of nonlinear interactions of $f+f = 2f$, $f+D_2 = fD_2$, and $D_1+D_2 = D_3$, respectively. No significant bicoherence values are found at $[f, D_1] = [0.485, 1.003]$ cpd. This suggests weak nonlinear interactions between near-inertial waves and diurnal tides ($f+D_1 = fD_1$), which is consistent with the weak fD_1 waves in Stage 2.

Figure 7b provides the bicoherence values with depth for the $[f, f]$, $[f, D_2]$, and $[D_1, D_2]$ frequency pairs. The bicoherence values at $[f, f]$ exceed the 90% statistical significance level between 60 and 90 m, suggesting that the superharmonic transfer of f energy to $2f$ ($\approx D_1$) mainly occurred in the upper ocean, which is consistent with the enhanced diurnal currents observed during Stage 2 (Figure 2b). The bicoherence values at $[f, D_2]$

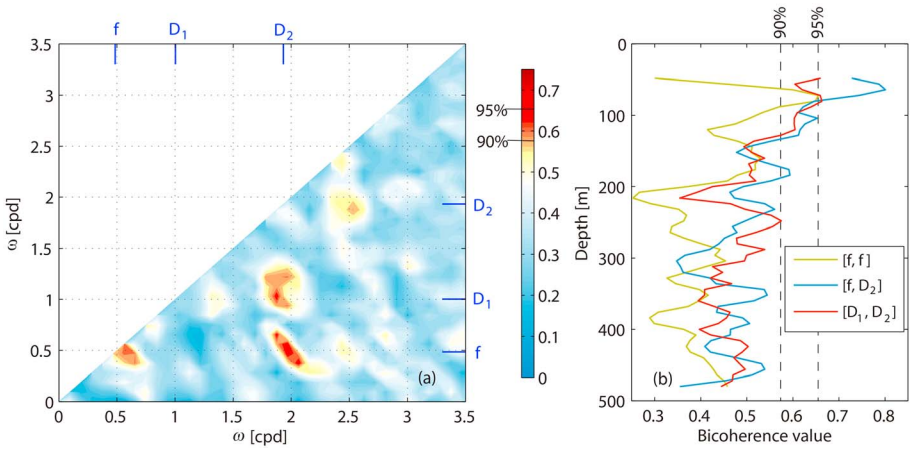

Figure 7. (a) Average bicoherence of the $u(t)$ and $v(t)$ velocities using data obtained between 72 and 96 m. The 90% and 95% statistical significance levels are indicated in the color bar. (b) Vertical profiles of bicoherence near the [f, f], [f, D_2], and [D_1, D_2] frequency pairs. The vertical dashed lines indicate the 90% and 95% statistical significance levels.

exceed the 90% statistical significance level in the upper 130 m, and even exceed the 95% statistical significance level in the upper 75 m, suggesting strong nonlinear interactions of f+$D_2 = fD_2$ in the upper ocean. This is consistent with the elevated fD_2 waves observed during Stage 2 (Figure 6b). Similarly, the bicoherence values exceeding the 90% statistical significance level at [D_1, D_2] suggest the occurrence of nonlinear interaction of D_1+$D_2 = D_3$ in the upper 130 m, which is consistent with the elevated D_3 waves presented in Figure 6e.

5. Discussion and Conclusions

Current data recorded from a moored ADCP in the western SCS were used to demonstrate the evolution of the internal wavefield and the enhancement of nonlinear interactions after the severe tropical storm Chanchu. The internal wavefield was characterized by semidiurnal and diurnal tides before the passage of Chanchu, whereas the internal wavefield after the passage of Chanchu was characterized not only by semidiurnal and diurnal tides but also by enhanced diurnal currents, fD_2 waves, and D_3 waves. Analysis of the shear spectra and rotary coefficient indicates that these observed waves were not spontaneously excited independent waves; they exhibited strong shear and were strongly related to the near-inertial waves and shear induced by Chanchu. These features are consistent with those of nonlinear coupling waves derived from nonlinear interactions. Analysis of the bicoherence further confirms that the enhanced diurnal currents, fD_2 waves, and D_3 waves were derived from the nonlinear interactions of f+$f = 2f$, f+$D_2 = fD_2$, and D_1+$D_2 = D_3$, respectively.

Nonlinear couplings between the wind-generated near-inertial waves and internal tides are common nonlinear processes in the ocean and have been reported in numerical experiments and observations (Davies & Xing, 2003; Guan et al., 2014; van Haren et al., 1999; Mihaly et al., 1998; Xing & Davies, 2002). However, to the best of our knowledge, no observations have reported the nonlinear interactions of f +$f = 2f$ and D_1+$D_2 = D_3$ after the passage of TCs. The occurrence of the nonlinear interactions of f+$f = 2f$ and D_1+$D_2 = D_3$ is a rare phenomenon, as either only near-inertial waves (f+$f = 2f$) or no near-inertial waves (D_1+$D_2 = D_3$) are involved in the interaction processes. Typically, external excited baroclinic waves are prone to couple with the existing internal waves, but it is difficult for them to undergo self-interactions or trigger nonlinear couplings between the existing internal waves. Thus, the nonlinear interactions of f +$f = 2f$ and D_1+$D_2 = D_3$ are rarely observed by mooring observations after the passage of TCs. In our observations, the location of the mooring might play an important role in the occurrence of these nonlinear interactions. Our mooring was located near the critical diurnal latitudes where $2f \approx D_1$. Near-inertial waves underwent self-interactions of f+$f = 2f$ in our observations, in which energy was transferred from near-inertial waves to their harmonic waves ($2f \approx D_1$). These harmonic waves further contributed to the nonlinear interactions of D_1+$D_2 = D_3$.

The occurrence of the self-interaction of near-inertial waves suggests that energy was transferred from the near-inertial waves to the diurnal waves, as our mooring was located near the critical diurnal latitudes where $2f \approx D_1$. These diurnal waves might contribute to the enhancement of diurnal currents observed in Stage 2. Using mooring data obtained from the northern SCS, Guan et al. (2014) also observed enhanced diurnal currents after the passage of typhoon Megi and attributed this enhancement to the intensification of stratification induced by Megi. Here there were no available temperature and salinity data during the observation period, and we cannot examine the impact of Chanchu on stratification. More observations or numerical experiments are required to further explore the enhancement of diurnal currents near the critical diurnal latitudes in the near future.

An interesting phenomenon observed here is that the nonlinear interactions between the near-inertial waves and diurnal tides ($f+D_1 = fD_1$) were weaker than the nonlinear interactions between near-inertial waves and semidiurnal tides ($f+D_2 = fD_2$), though the diurnal tides were 5 times stronger than the semidiurnal tides after the passage of Chanchu. This is contrary to the observations reported by Guan et al. (2014), who found strong nonlinear interactions of $f+D_1 = fD_1$ but weak nonlinear interactions of $f+D_2 = fD_2$ after the passage of typhoon Megi in the northern SCS. We expect that various factors contribute to this difference, which may include the critical diurnal latitudes. Near-inertial waves underwent self-interactions near the critical diurnal latitudes, involving energy transfer from the near-inertial to diurnal waves. This process might affect the nonlinear interactions between near-inertial waves and diurnal tides. However, more observations or numerical experiments are required to investigate these processes.

This study provides a suggestive and intriguing insight into the effect of TCs on the internal wavefield and nonlinear interactions in the western SCS. A dozen TCs pass through or form in the SCS each year, many of which propagate across the critical diurnal latitudes and induce strong near-inertial waves. Our observations suggest that, in addition to the nonlinear interactions between near-inertial waves and internal tides, the TC-induced near-inertial energy near the critical diurnal latitudes can also be cascaded into high-frequency internal waves through the nonlinear interactions of $f+f = 2f$ and $D_1+D_2 = D_3$, which are rarely observed in regions far away from the critical diurnal latitudes. These nonlinear processes would greatly promote the cascade of near-inertial energy and suggest strong turbulent mixing near the critical diurnal latitudes. However, our research is a case study. More observations or numerical experiments are required to further investigate the influence of critical diurnal latitudes on nonlinear processes in the near future.

Acknowledgments
This work is supported by the National Natural Science Foundation of China (41630970, 41676022, 41876022, 41876023, 41806033, and 41521005) and the Open Project Program of State Key Laboratory of Tropical Oceanography (LTOZZ1801). The data we used are from the South China Sea Institute of Oceanology, Chinese Academy of Sciences, and available at https://jmp.sh/JvwVVtv.

References

Alford, M. H. (2001). Fine-structure contamination: Observations and a model of a simple two-wave case. *Journal of Physical Oceanography*, *31*(9), 2645–2649. https://doi.org/10.1175/1520-0485(2001)031<2645:Fscoaa>2.0.Co;2

Alford, M. H. (2008). Observations of parametric subharmonic instability of the diurnal internal tide in the South China Sea. *Geophysical Research Letters*, *35*, L15602. https://doi.org/10.1029/2008GL034720

Alford, M. H., MacKinnon, J. A., Zhao, Z. X., Pinkel, R., Klymak, J., & Peacock, T. (2007). Internal waves across the Pacific. *Geophysical Research Letters*, *34*, L24601. https://doi.org/10.1029/2007GL031566

Cao, A., Guo, Z., Song, J., Lv, X., He, H., & Fan, W. (2018). Near-inertial waves and their underlying mechanisms based on the South China Sea internal wave experiment (2010–2011). *Journal of Geophysical Research: Oceans*, *123*, 5026–5040. https://doi.org/10.1029/2018JC013753

Chen, G., Xue, H., Wang, D., & Xie, Q. (2013). Observed near-inertial kinetic energy in the northwestern South China Sea. *Journal of Geophysical Research: Oceans*, *118*, 4965–4977. https://doi.org/10.1002/jgrc.20371

D'Asaro, E. A. (1989). The decay of wind-forced mixed layer inertial oscillations due to the β effect. *Journal of Geophysical Research*, *94*(C2), 2045–2056. https://doi.org/10.1029/JC094iC02p02045

Davies, A. M., & Xing, J. X. (2003). On the interaction between internal tides and wind-induced near-inertial currents at the shelf edge. *Journal of Geophysical Research*, *108*(C3), 3099. https://doi.org/10.1029/2002JC001375

Elgar, S., & Guza, R. T. (1988). Statistics of bicoherence. *IEEE Transactions on Acoustics, Speech, and Signal Processing*, *36*(10), 1667–1668. https://doi.org/10.1109/29.7555

Ferrari, R., & Wunsch, C. (2009). Ocean circulation kinetic energy: Reservoirs, sources, and sinks. *Annual Review of Fluid Mechanics*, *41*(1), 253–282. https://doi.org/10.1146/annurev.fluid.40.111406.102139

Garrett, C. (2001). What is the "near-inertial" band and why is it different from the rest of the internal wave spectrum? *Journal of Physical Oceanography*, *31*(4), 962–971. https://doi.org/10.1175/1520-0485(2001)031<0962:Witnib>2.0.Co;2

Garrett, C., & Munk, W. (1975). Space-time scales of internal waves-progress report. *Journal of Geophysical Research*, *80*(3), 291–297. https://doi.org/10.1029/Jc080i003p00291

Garrett, C., & Munk, W. (1979). Internal waves in the ocean. *Annual Review of Fluid Mechanics*, *11*(1), 339–369. https://doi.org/10.1146/annurev.fl.11.010179.002011

Gill, A. E. (1984). On the behavior of internal waves in the wakes of storms. *Journal of Physical Oceanography*, *14*(7), 1129–1151. https://doi.org/10.1175/1520-0485(1984)014<1129:Otboiw>2.0.Co;2

Goh, A. Z. C., & Chan, J. C. L. (2010). Interannual and interdecadal variations of tropical cyclone activity in the South China Sea. *International Journal of Climatology*, *30*(6), 827–843.
Gonella, J. (1972). A rotary-component method for analysing meteorological and oceanographic vector time series. *Deep-Sea Research*, *19*(12), 833–846. https://doi.org/10.1016/0011-7471(72)90002-2
Guan, S., Zhao, W., Huthnance, J., Tian, J., & Wang, J. (2014). Observed upper ocean response to typhoon Megi (2010) in the northern South China Sea. *Journal of Geophysical Research: Oceans*, *119*, 3134–3157. https://doi.org/10.1002/2013JC009661
Kim, Y. C., & Powers, E. J. (1978). Digital bispectral analysis of self-excited fluctuation spectra. *Physics of Fluids*, *21*(8), 1452–1453. https://doi.org/10.1063/1.862365
Kim, Y. C., & Powers, E. J. (1979). Digital bispectral analysis and its applications to non-linear wave interactions. *IEEE Transactions on Plasma Science*, *7*(2), 120–131. https://doi.org/10.1109/Tps.1979.4317207
Mihaly, S. F., Thomson, R. E., & Rabinovich, A. B. (1998). Evidence for nonlinear interaction between internal waves of inertial and semidiurnal frequency. *Geophysical Research Letters*, *25*(8), 1205–1208. https://doi.org/10.1029/98GL00722
Oey, L. Y., Inoue, M., Lai, R., Lin, X. H., Welsh, S. E., & Jr, L. J. R. (2008). Stalling of near-inertial waves in a cyclone. *Geophysical Research Letters*, *35*, L12604. https://doi.org/10.1029/2008GL034273
Qi, H., De Szoeke, R. A., Paulson, C. A., & Eriksen, C. C. (1995). The structure of near-inertial waves during ocean storms. *Journal of Physical Oceanography*, *25*(11), 2853–2871. https://doi.org/10.1175/1520-0485(1995)025<2853:TSONIW>2.0.CO;2
Sanford, T. B., Price, J. F., & Girton, J. B. (2011). Upper-ocean response to Hurricane Frances (2004) observed by Profiling EM-APEX floats. *Journal of Physical Oceanography*, *41*(6), 1041–1056.
Sanford, T. B., Price, J. F., Girton, J. B., & Webb, D. C. (2007). Highly resolved observations and simulations of the ocean response to a hurricane. *Geophysical Research Letters*, *34*, L13604. https://doi.org/10.1029/2007GL029679
Simmons, H. L. (2008). Spectral modification and geographic redistribution of the semi-diurnal internal tide. *Ocean Modelling*, *21*(3-4), 126–138. https://doi.org/10.1016/j.ocemod.2008.01.002
Sun, L., Zheng, Q. A., Wang, D. X., Hu, J. Y., Tai, C. K., & Sun, Z. Y. (2011). A case study of near-inertial oscillation in the South China Sea using mooring observations and satellite altimeter data. *Journal of Oceanography*, *67*(6), 677–687. https://doi.org/10.1007/s10872-011-0081-9
Teague, W. J., Jarosz, E., Wang, D. W., & Mitchell, D. A. (2007). Observed oceanic response over the upper continental slope and outer shelf during Hurricane Ivan. *Journal of Physical Oceanography*, *37*(9), 2181–2206.
Thomson, R. E., & Emery, W. J. (2014). *Data analysis methods in physical oceanography*. Oxford, UK: Newnes.
van Haren, H. (2003). On the polarization of oscillatory currents in the Bay of Biscay. *Journal of Geophysical Research*, *108*(C9), 3290. https://doi.org/10.1029/2002JC001736
van Haren, H., Maas, L., & van Aken, H. (2002). On the nature of internal wave spectra near a continental slope. *Geophysical Research Letters*, *29*(12), 1615. https://doi.org/10.1029/2001GL014341
van Haren, H., Maas, L., Zimmerman, J. T. F., Ridderinkhof, H., & Malschaert, H. (1999). Strong inertial currents and marginal internal wave stability in the central North Sea. *Geophysical Research Letters*, *26*(19), 2993–2996. https://doi.org/10.1029/1999GL002352
Wang, G., Su, J., Ding, Y., & Chen, D. (2007). Tropical cyclone genesis over the South China Sea. *Journal of Marine Systems*, *68*(3-4), 318–326. https://doi.org/10.1016/j.jmarsys.2006.12.002
Xie, X. H., Chen, G. Y., Shang, X. D., & Fang, W. D. (2008). Evolution of the semidiurnal (M-2) internal tide on the continental slope of the northern South China Sea. *Geophysical Research Letters*, *35*, L13604. https://doi.org/10.1029/2008GL034179
Xie, X. H., Shang, X. D., Chen, G. Y., & Sun, L. (2009). Variations of diurnal and inertial spectral peaks near the bi-diurnal critical latitude. *Geophysical Research Letters*, *36*, L02606. https://doi.org/10.1029/2008GL036383
Xing, J. X., & Davies, A. M. (2002). Processes influencing the non-linear interaction between inertial oscillations, near inertial internal waves and internal tides. *Geophysical Research Letters*, *29*(5), 1067. https://doi.org/10.1029/2001GL014199
Xu, Z. H., Yin, B. S., Hou, Y. J., & Xu, Y. S. (2013). Variability of internal tides and near-inertial waves on the continental slope of the northwestern South China Sea. *Journal of Geophysical Research: Oceans*, *118*, 197–211. https://doi.org/10.1029/2012JC008212